

Coordinating Anions “to the Rescue” of the Lithium Ion Mobility in Ternary Solid Polymer Electrolytes Plasticized With Ionic Liquids

Jan-Philipp Hoffknecht, Alina Wettstein, Jaschar Atik, Christian Krause, Johannes Thienenkamp, Gunther Brunklaus, Martin Winter, Diddo Diddens,* Andreas Heuer,* and Elie Paillard*


Lithium salts with low coordinating anions such as bis(trifluoromethanesulfonyl)imide (TFSI) have been the state-of-the-art for polyethylene oxide (PEO)-based “dry” polymer electrolytes for 3 decades. Plasticizing PEO with TFSI-based ionic liquids (ILs) to form ternary solid polymer electrolytes (TSPEs) increases conductivity and Li⁺ diffusivity. However, the Li⁺ transport mechanism is unaffected compared to their “dry” counterparts and is essentially coupled to the dynamics of the polymer host matrix, which limits Li⁺ transport improvement. Thus, a paradigm shift is hereby suggested: the utilization of more coordinating anions such as trifluoromethanesulfonyl-*N*-cyanoamide (TFSAM), able to compete with PEO for Li⁺ solvation, to accelerate the Li⁺ transport and reach a higher Li⁺ transference number. The Li–TFSAM interaction in binary and ternary TFSAM-based electrolytes is probed by experimental methods and discussed in the context of recent computational results. In PEO-based TSPEs, TFSAM drastically accelerates the Li⁺ transport (increases Li⁺ transference number by a factor 6 and the Li⁺ conductivity by 2–3) and computer simulations reveal that lithium dynamics are effectively re-coupled from polymer to anion dynamics. Last, this concept of coordinating anions in TSPEs is successfully applied in LFP||Li metal cells leading to enhanced capacity retention (86% after 300 cycles) and an improved rate performance at 2C.

1. Introduction

“Dry” polyethylene oxide (PEO)-based electrolytes, made of a lithium salt dissolved in a polymer matrix, are the current state-of-the-art “dry” solid polymer electrolytes (SPEs).^[1] They reach ionic conductivities $\approx 10^{-4}$ S cm⁻¹ at 40 °C, thanks to the strategies that have been developed to suppress the crystallinity of linear PEOs and their crystalline complexes (i.e., crosslinking, statistical copolymers, and “plasticizing” lithium salts).^[2] However, for a use in automotive batteries, conductivities around 10⁻³ S cm⁻¹ and higher are necessary, which implies an operational temperature above 60 °C for the present level of development of lithium metal polymer batteries (LMPBs). One strategy for decreasing the operation temperature of SPEs has been the use of plasticizers yielding ternary SPEs (TSPEs), with a higher segmental mobility and faster ionic transport.^[3,4] Among the proposed compounds, ionic liquids (ILs) present the significant advantage of being non-volatile

J.-P. Hoffknecht
Institute for Inorganic and Analytical Chemistry
University of Münster
Corrensstrasse 28/30, D48149 Münster, Germany
J.-P. Hoffknecht, C. Krause, M. Winter
MEET Battery Research Center
University of Münster
Corrensstrasse 46, D48149 Münster, Germany

A. Wettstein, A. Heuer
Institute for Physical Chemistry
University of Münster
Corrensstrasse 28/30, D48149 Münster, Germany
E-mail: a.heuer@fz-juelich.de
J. Atik, J. Thienenkamp, G. Brunklaus, M. Winter, D. Diddens,
A. Heuer, E. Paillard
Helmholtz Institute Münster – Forschungszentrum Jülich GmbH
(IEK 12)
Corrensstrasse 46, D48149 Münster, Germany
E-mail: d.diddens@fz-juelich.de; elielisee.paillard@polimi.it
E. Paillard
Department of Energy
Politecnico di Milano
via Lambruschini 4, Milan 20148, Italy

 The ORCID identification number(s) for the author(s) of this article can be found under <https://doi.org/10.1002/aenm.202202789>.

© 2022 The Authors. Advanced Energy Materials published by Wiley-VCH GmbH. This is an open access article under the terms of the Creative Commons Attribution License, which permits use, distribution and reproduction in any medium, provided the original work is properly cited.

DOI: 10.1002/aenm.202202789

and non-flammable in most circumstances.^[5–8] A common design rule for ILs is to combine a low coordinating anion with an organic cation, such as a tetra-alkyl ammoniums. Low coordinating anions such as PF₆[−], bis(trifluoromethanesulfonyl) imide (TFSI), or bis(fluorosulfonyl)imide (FSI) are typically used in lithium-ion and lithium metal battery electrolytes. In fact, organic and very weakly coordinating anions such as TFSI were first proposed for “dry” SPEs.^[9] Indeed, although PEO possesses a high donor number which favors the solvation of lithium and thereby promotes the solubility of lithium salts, its dielectric constant is relatively low. Hence, low coordinating anions such as TFSI result in easily soluble, low lattice energy lithium salts that reach the highest dissociation and the best conductivities in “dry” SPEs. However, these anions do not interact much with the PEO matrix nor Li⁺; and thus, do not compete with the strong Li⁺ coordination by the PEO segments. As a result, their mobility is much higher than that of the Li⁺ cation, which results in lithium transference numbers (*t*_{Li⁺}) relatively low versus liquid electrolytes.^[10,11] For instance, PEO/LiTFSI complexes achieve *t*_{Li⁺} of ≈0.1–0.15^[12,13] as opposed to ≈0.3–0.4 for liquid, alkyl carbonate-based electrolytes.^[14] Adding an ionic liquid allows preparing ternary solid polymer electrolytes with considerably improved conductivity at 40 °C (up to 10^{−3} S cm^{−1}).^[15] Nevertheless, the introduction of extra ions in the form of ILs results in a further decrease of *t*_{Li⁺}. In fact, although binary Li salt/ILs binary mixtures allow solvation and transport of Li⁺, it has been shown that an IL such as *N*-butyl-*N*-methyl pyrrolidinium (PYR₁₄) TFSI acts strictly as a plasticizer and that its effect is mainly linked to an acceleration of PEO-related conduction modes rather than inducing new conduction modes because it does not compete significantly with PEO for Li⁺ solvation. The main transport mode is along the PEO chain (intrachain transport), and thus adding the IL “disperse” Li⁺ conduction pathways.^[16]

Thus, considering that, for different ILs with the same cation, viscosity and conductivity are more linked to the size of the anion than to its coordinating ability,^[17] it seems promising to use ILs with lower viscosity to reach a stronger plasticizing effect. Besides, it can be advantageous to introduce other coordinating groups into the system in order to enable additional conduction pathways for Li⁺ rather than only accelerating PEO own conduction modes. For instance, we showed recently that, by use of ILs with a coordinating cation (i.e., a TFSI-based IL with a pyrrolidinium cation bearing a short PEO chain long enough to solvate a single Li⁺ cation), it was possible to triple the transference number of TSPEs compared to an alkyl-substituted IL counterpart.^[13,18] However, it must be pointed out that the IL is extremely viscous. Moreover, a part of its plasticizing effect at a given molar fraction originates from its very high molecular weight (given that the *T*_g of a mixture of two compounds *a* and *b* scales with mass fractions according to the Flory–Fox law (i.e., 1/*T*_{g,ab} = *x*_a/*T*_{g,a} + *x*_b/*T*_{g,b}), with *x*_a and *x*_b, the mass fractions of each compounds).^[19]

Departing from the strategy of coordinating cations, we report here an approach based on solvating anions, employing a recently reported IL made of an anion recently proposed for IL-based electrolytes, trifluoromethanesulfonyl-*N*-cyanoamide (TFSAM). This anion is a hybrid between TFSI and dicyanoamide (DCA) as its negative charge is delocalized on one

side within the −SO₂CF₃ strongly electron-withdrawing group, and on the other side, by a −CN group. Compared to the SO₂CF₃, the −CN group is not only slightly less electronegative but also more polar and more coordinating itself. This anion, stable to hydrolysis, is asymmetric, which allows obtaining fully amorphous ILs and Li⁺ electrolytes. Its anodic stability, although slightly lower than that of TFSI, is sufficient for the application and, contrary to TFSI, it presents the added benefit of not inducing any anodic dissolution of aluminum current collector at high voltage, even in carbonate-based lithium-ion battery electrolytes.^[20,17]

We show here in a combined experimental and computational study that, contrary to the common approach of using ILs that comprise the most weakly coordinating anions which perform best in “dry” binary SPEs or liquid electrolytes, using a smaller and more coordinating anion is beneficial in the framework of TSPEs. Recently, we suspected a similar effect (although to a lesser extent) induced by the fluorine-free 4,5-dicyano-1,2,3-triazolate (DCTA) anion. However, in this case, it could only partially counterbalance the much lower conductivity versus the TFSI analog, and Li metal cells had a lower performance.^[21] With TFSAM, the new “anion-assisted” Li⁺ transport mechanism allows a drastically faster Li⁺ transport in TSPEs compared to the TFSI analog. This leads to an improved rate performance of LMPBs and an enhanced capacity retention of LMPBs in the long-term as well.

2. Results

2.1. Fundamental Understanding of the Unique Li–TFSAM Interaction in ILs

As mentioned above, the TFSAM anion is utilized to enhance the Li⁺ mobility in TSPEs via a novel “anion-assisted” transport mechanism. Nevertheless, to fully understand this new transport mode, it is necessary to take a step back and investigate the interaction of Li⁺ with asymmetric anions such as TFSAM in a more simplified system (than in the TSPE). Here, the system of choice is the binary mixture of an IL and the corresponding lithium salt to gain a fundamental understanding first.

Regarding the Li⁺ coordination by anions with different functional groups, it has been reported that in IL mixtures including TFSI and DCA, the CN-group of DCA is the preferred coordination site.^[22] Recently, Nürnberg et al. reported that, at concentrations of LiTFSAM below 30 mol%, only Li–CN coordination is observable via Raman and NMR spectroscopy and that this Li–anion interaction is stronger compared to that of Li–TFSI.^[23] A recent computational counterpart study confirmed that only in the regime of high salt concentrations when coordination can no longer be afforded by the preferred cyano-group, new binding geometries, for example, to the eq sulfonyl oxygens or even to the center nitrogen, emerge.^[24]

To complete the picture, here, TFSAM containing electrolytes are compared to both of its structurally related symmetric anions (TFSI and DCA, see **Figure 1**). To precisely observe any effects on Li–anion interaction, a comparative study with IL-based electrolytes with incremental increases of lithium salt fractions (0–12.5 mol%) is performed. In the following combined physicochemical and electrochemical study, the

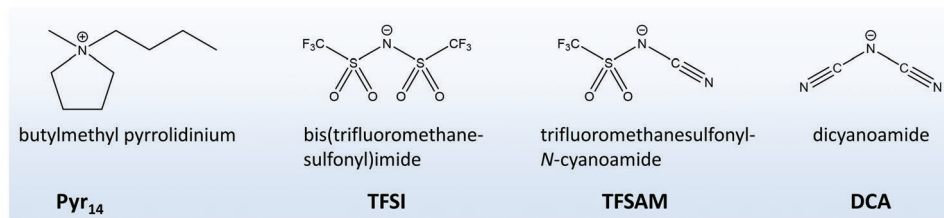


Figure 1. Molecular structures of butylmethyl pyrrolidinium (Pyr₁₄), bis(trifluoromethanesulfonyl)imide (TFSI), trifluoromethanesulfonyl-*N*-cyanoamide (TFSAM), and dicyanoamide (DCA).

unique Li–TFSAM interaction is highlighted in IL-based electrolytes, which grants a proper background to understand the change in Li⁺ transport, when TFSAM is utilized in TSPEs later.

2.2. TFSAMs Effect on Viscosity, Ionic Conductivity, and Li⁺ Diffusion

As reported earlier,^[17] the viscosities of the pure ILs, Pyr₁₄DCA, Pyr₁₄TFSAM, and Pyr₁₄TFSI scale with the size of the anion, that is, with the larger anions leading to higher viscosities, as in ILs the molecular radius of the ions usually affects the shear resistance (and therefore the viscosity) to a much greater extent than the interactions between the Pyr₁₄⁺ cation and the anion.^[25–27] This behavior changes when lithium ions are introduced in the system. As can be seen in **Figure 2a**, the introduction of the lithium salt has a higher influence on the viscosities of TFSAM-based binary electrolytes than on either TFSI or DCA-based ones. At low salt contents, the viscosity curves still follow the previous trend, that is, increase according to anion size. This changes with higher fractions of Li⁺ and, at 12.5 mol%, the TFSAM-based electrolyte even surpasses its TFSI counterpart. The strong interaction between Li⁺ and TFSAM[−], leading to increased shear resistance, is a possible explanation, which is further corroborated by the quite different coordination shell sizes observed in molecular dynamics (MD) simulations.^[24] Although, on average, three TFSI molecules closely entwine themselves around the lithium ion in a preferably bidentate binding geometry, four TFSAM anions create an extended solvation sphere through solely mono-dentate cyano-contacts.

A similar trend is observed for the ionic conductivity of these binary electrolytes (**Figure 2b**). A drop of conductivity upon adding a lithium salt is typical for IL-based electrolytes^[28–30] as the Li–anion interaction is stronger than the interaction between the anion and Pyr₁₄⁺ (sterically and electronically hindered: +*I* effect of the alkyl chains). Here also, the Li⁺ coordination by TFSAM seems particularly high. It has already been reported that, for TFSAM, the decrease of conductivity with increasing salt concentration is more severe (compared to TFSI)^[23] due to the higher ion–ion interaction because of the Li–CN coordination in the case of TFSAM. Thus, one could have expected that within the series of TFSI, TFSAM, and DCA, the DCA-based electrolytes would have shown the highest conductivity drop with salt addition, given the presence of two –CN groups on the anion. However, this is not the case. As is visualized more clearly in **Figure 2c**, the TFSAM-based electrolytes show the highest relative drop in conductivity compared to the corresponding pure IL.

This behavior is logically also reflected in the Li⁺ diffusion coefficients, which were determined by PFG-NMR for these binary electrolytes (**Figure 2d**). Interestingly, the TFSAM-based electrolytes reach values close to TFSI-based ones at 75 mol% salt content; although, at this concentration, the TFSAM electrolyte has a higher conductivity and a lower viscosity. Thus, a hindered Li⁺ transport due to its strong coordination by TFSAM can be assumed for these binary mixtures. The introduction of the stronger coordinating CN-group seems to have a more pronounced effect in the case of TFSAM compared to DCA, which might be counter-intuitive at first. However, the difference is that DCA offers two equally favored coordination sites for Li⁺ as the electron density of the negative charge can be delocalized over the two CN-groups of DCA (see **Figure S3**, Supporting Information, for mesomeric structures); the Li–DCA interaction of an existing ion pair would be weakened as soon as another Li⁺ approaches the opposite CN-group, leading to an overall faster ion exchange. On the other hand, with TFSAM, this is less likely to happen because the CN-coordination site of TFSAM is electronically more favored than the Li⁺-interaction with an oxygen of the –SO₂CF₃ group. Furthermore, the size difference might play a role with the small DCA anion moving faster from the solvation sphere. Thus, it can be stated that the asymmetric combination of electron-withdrawing groups creates in the case of TFSAM, an “anomaly” within the series of TFSI, TFSAM and DCA in terms of Li–anion interaction.

To conclude, the investigation of the binary systems supports the expected strong Li–anion interaction for TFSAM with a preferred Li–CN coordination. In addition, the direct comparison with the two related symmetric anions (TFSI and DCA) also reveals that it is not only because the Li–CN coordination is “naturally” stronger than the Li–O. Instead, the asymmetric combination with a weaker coordination side (–SO₂CF₃) leads to an even more pronounced Li–TFSAM interaction on the CN-site. In the case of binary liquid electrolytes, this has a negative effect on Li⁺ transport in view of battery application.

However, in the following, this marked coordination is utilized to shift the Li⁺ coordination and transport in PEO-based electrolytes from polymer to anion dominance and the binary (IL-based) systems results grant support for the understanding of the transport mechanism in TSPEs.

2.3. TFSAM in Ternary Solid Polymer Electrolytes

TFSAM with its strong unilateral Li⁺ coordination was selected for a new class of TSPEs, where the IL does not act only as

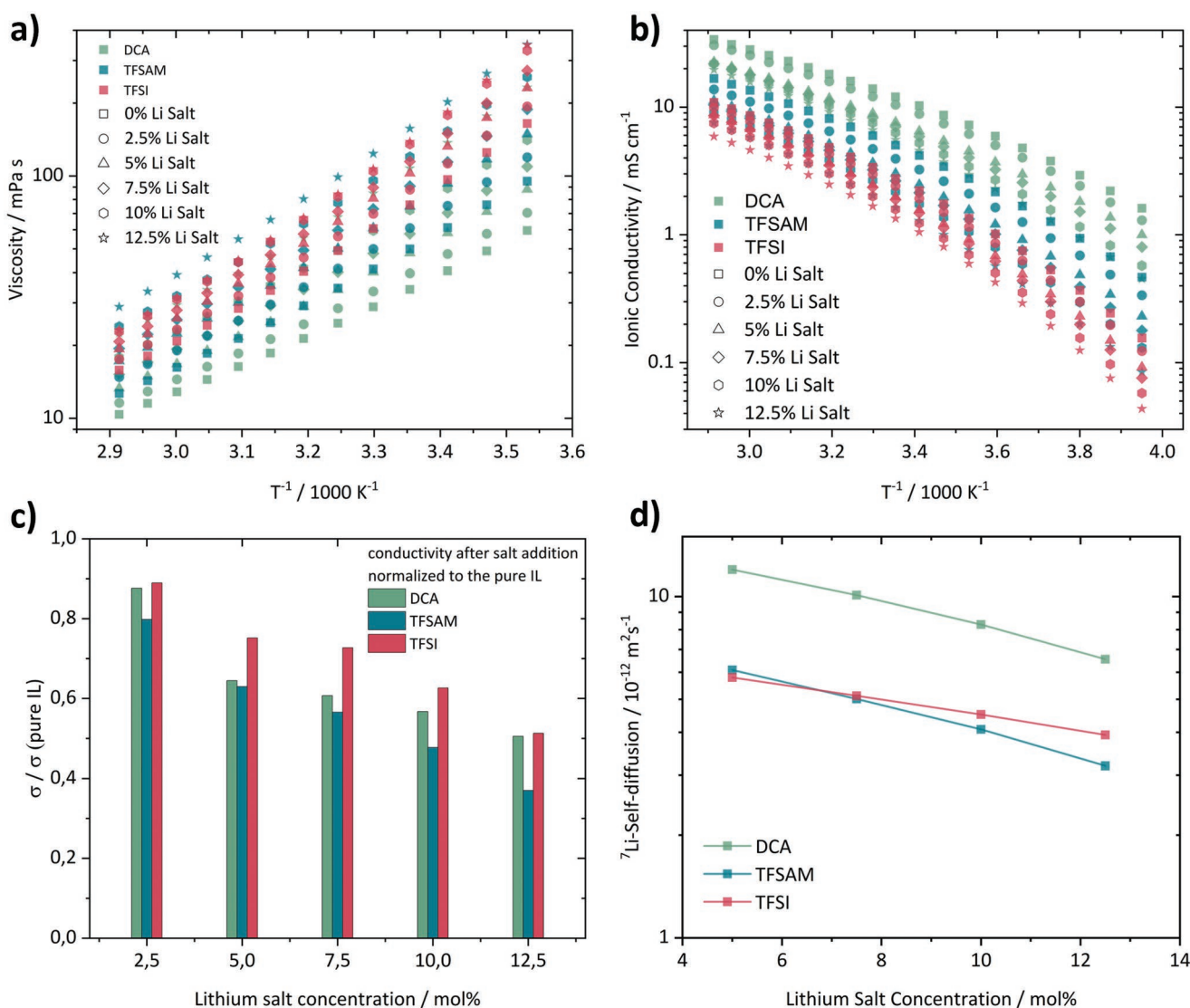


Figure 2. a) Viscosities of the binary IL-based electrolytes depending on temperature (10–70 °C) and lithium salt concentration (0–12.5 mol%); b) ionic conductivities of the binary IL-based electrolyte depending on temperature (–20–70 °C) and lithium salt concentration (0–12.5 mol%); c) drop of conductivity with addition of lithium salt; ionic conductivities of binary IL-based electrolytes divided by the conductivity of the pure IL; exemplarily shown for 40 °C; d) concentration dependent Li^+ diffusion coefficients determined via PFG-NMR at 25 °C.

plasticizer but also at the same time, can “free” the Li^+ from the strong coordinating PEO chain, and thereby, accelerate Li^+ transport. Thus, TFSAM-based TSPE membranes with several PEO:salt:IL ratios were prepared by a solvent-free processing and investigated. They were compared to state-of-the-art TFSI-based TSPEs in terms of transport properties and, with the support of MD simulations, a new “anion-assisted” transport mechanism was proposed (DCA-based TSPEs could not be prepared due to the phase separation of IL and PEO).

2.4. Thermal Behavior and Li^+ Coordination Environment

The thermal behavior of TFSI- and TFSAM-based polymer electrolytes was investigated via differential scanning calorimetry (DSC). Thus, membranes with a favorable PEO:salt:IL ratio (in

terms of crystallinity) can be preselected. At the same time, the glass transition temperatures (T_g) of the membranes grant first insights on potential difference in terms of segmental mobility.

The DSC heating scans of the TSPEs are presented in **Figure 3a** (heating scan after a quenching step shown; following cooling scan: see Supporting Information). There are only minor differences in the crystallization and melting behavior between TFSI and TFSAM-based membranes; although, it is noticeable that TFSI-based membranes tend to stay more amorphous as seen from the smaller or non-existent cold-crystallization and melting peaks. This is expected because TFSI is the lower coordinating anion, so, it can be considered fully dissociated in the PEO-matrix, whereas the TFSAM anion; although asymmetric, likely suffers from its stronger interaction with Li^+ that helps the formation of crystalline complexes from the stronger solvation structures in solution. In general,

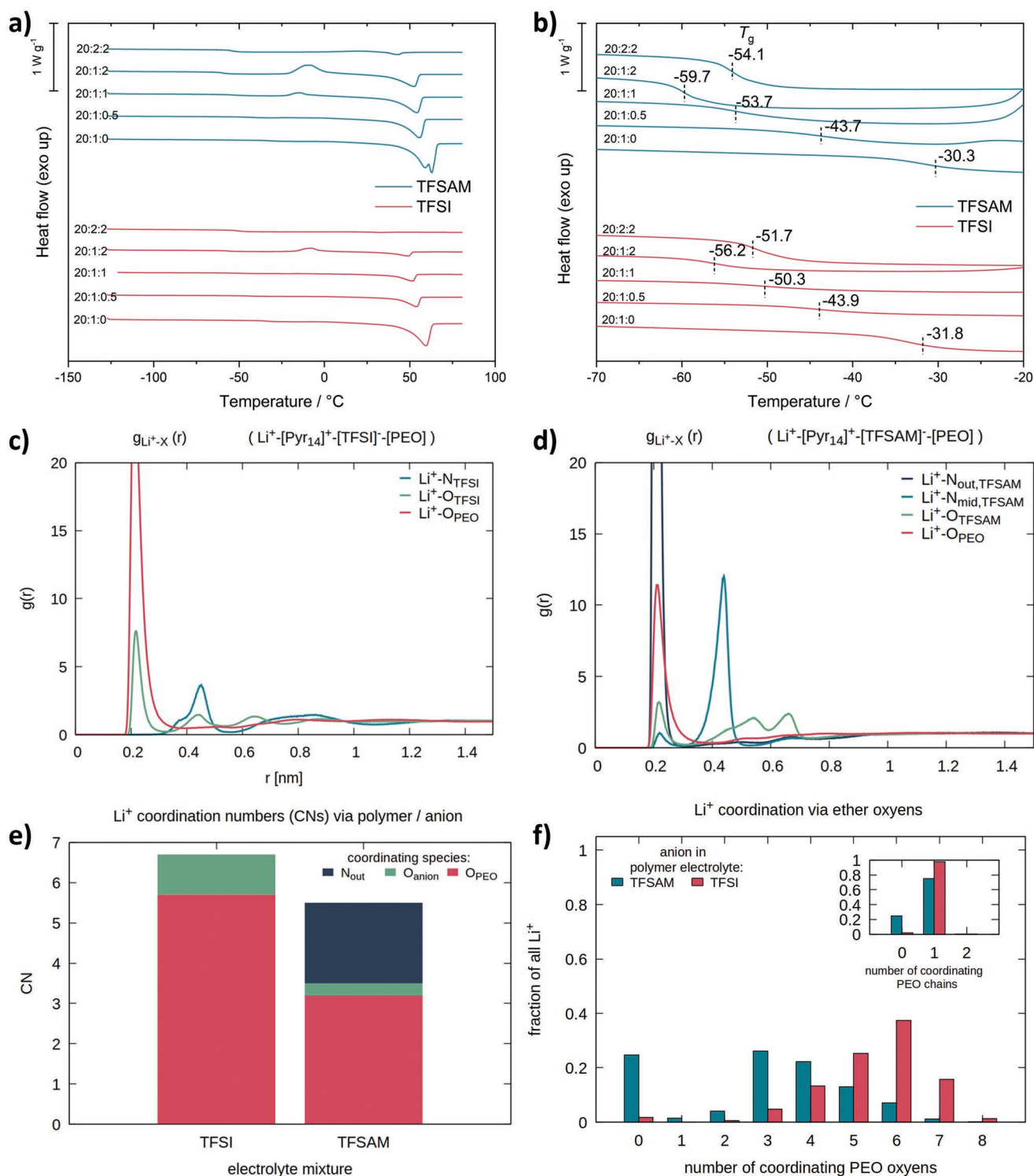


Figure 3. Top row a,b): DSC thermograms of TFSAM and TFSI-based ternary electrolytes with different PEO:salt:IL ratios; scan rate: $5\text{ }^\circ\text{C min}^{-1}$; shown: heat ramp after quenching step; middle row: coordination environment of the lithium ion displayed via radial distribution functions $g_{Li^+-X}(r)$ between lithium ions and binding sites provided by the polymer chains and the respective anion, that is, c) TFSI and d) TFSAM; e) composition of lithium coordination shell in terms of ether oxygen and anion coordination numbers CN; f) probability distribution of Li^+-O_{PEO} coordination numbers regardless if the ether oxygens are provided by a single or multiple PEO chains. The inset shows the probability to find Li^+ bound to one or two PEO chains or structurally decoupled from the polymer (0).

for both anions, a PEO:salt ratio of 20:2 seems to be beneficial to reduce the crystallinity.

Besides crystallinity, the evolution of the T_g is of high interest for polymer electrolytes, as a lower T_g usually represents a higher segmental mobility of the polymer chains at a given temperature; hence, a faster Li^+ transport. With the first addition of lithium salt (see 20:1:0 membranes in Figure 3b), the usual increase in T_g (compared to pure PEO: $-52\text{ }^\circ\text{C}^{[31]}$) is observed as the Li^+ coordination by the ether oxygens of the PEO “stiffens” the polymer chains. After that, the addition of IL seems to have the usual plasticizing effect of increasing the segmental mobility again (seen as lowering the T_g). Interestingly, the use of $\text{Pyr}_{14}\text{TFSAM}$ leads to slightly lower T_g than $\text{Pyr}_{14}\text{TFSI}$, at least for the two sets of membranes that are fully amorphous when passing their T_g (20:1:2 and 20:2:2). $\text{Pyr}_{14}\text{TFSAM}$ seems to be a better plasticizer in these cases compared to $\text{Pyr}_{14}\text{TFSI}$, despite the higher viscosity of liquid TFSAM-based electrolytes at high salt ratios. The more likely explanation is that, due to the introduction of the coordinating TFSAM anion, the coordination of Li^+ by PEO (and its influence on increasing the T_g) is affected.

The molecular resolution of the MD simulations provides the opportunity to elucidate the lithium coordination behavior in the TFSI and TFSAM-containing membranes for qualitative differences. The solvation environment of the lithium ions is analyzed by means of radial distribution functions (RDFs) $g_{\text{Li}^+-X}(r)$ between lithium and the possible binding sites X offered by the polymer and the anions (Equation (1)):

$$g_{\text{Li}^+-X}(r) = \frac{V}{4\pi r^2 N_{\text{Li}^+} N_X} \left\langle \sum_i^{N_{\text{Li}^+}} \sum_j^{N_X} \delta(r - |\bar{r}_i - \bar{r}_j|) \right\rangle \quad (1)$$

where V corresponds to the volume of the simulation cell, and N_{Li^+} and N_X denote the number of atoms of the respective species. In principle, the RDF probes the probability to encounter species X within a distance r of a distinct Li^+ . Figure 3c,d depicts the arrangement of the polymer ether oxygens O_{PEO} and the anions around lithium. To probe both the number of coordination contacts and the binding geometry, that is, monodentate versus bidentate, the TFSI coordination is tracked by its O_{TFSI} atoms as well as N_{TFSI} . As previously discussed, TFSAM provides a cyano-nitrogen as an additional, and most favorable, coordination site which is termed $N_{\text{out,TFSAM}}$ opposed to the central nitrogen $N_{\text{mid,TFSAM}}$ which is also contained in TFSI.

In both electrolyte mixtures, we observe sharp coordination peaks at a distance of 2 Å, which therefore describe the compositions of the first coordination sphere. In the TFSI-containing electrolyte, lithium is primarily solvated by the ether oxygens but also shows contributions from O_{TFSI} . Unlike in the pure IL scenario, the latter binds to lithium in a monodentate manner which can be deduced from the split peak structure of $\text{Li}^+ - N_{\text{mid,TFSAM}}$ RDF with the right shoulder being more populated.

In accordance with previous experimental and theoretical studies involving cyano-moieties in competition with other Li^+ coordination sites such as O_{PEO} or O_{TFSI} ,^[22,23,24,32] we find that the $N_{\text{out,TFSAM}}$ coordination peak superimposes that of the ether oxygens, with the latter being downsized significantly in reference to the TFSI analog mixture. We can thus infer that

lithium coordination by the polymer chain is partially superseded by TFSAM.

The coordination numbers (CNs) are computed by integrating $g_{\text{Li}^+-X}(r)$ up to the position of the first minimum r_{min} (Equation (2)):

$$\text{CN} = 4\pi\rho_{X,\text{bulk}} \int_0^{r_{\text{min}}} dr r^2 g_{\text{Li}^+-X}(r) \quad (2)$$

The average composition of a lithium solvation shell in both electrolytes is compared in Figure 3e and visualized in snapshots in Figure 4.

Figure 3f shows the distribution of coordinated PEO oxygens in Li^+ solvation sphere and the inset details the number of PEO chains involved in the solvation. In good agreement with a recent simulation study employing a polarizable force field of a similar system composition (10:1:2),^[33] we observe for the TFSI-containing mixture, a distribution of coordination motifs involving 4–7 ether oxygens, which are almost exclusively provided by a single PEO-strand. Deviating from this simulation study, we find a statistically more frequent additional coordination via one TFSI oxygen on average (Figure 3e). Despite scaling the atomic partial charges, the strength of ionic interactions may still be slightly overestimated and the cause for such discrepancies. For the polymer electrolyte comprising the TFSAM anion on the other hand, the coordination shell is considerably downsized. First, the absolute number of atomic species that are bound to lithium reduces from 6.7 in the TFSI analog to 5.5 (see Figure 3e) of which only ≈ 3 monomer units account for the structural attachment of lithium to the polymer chains. Instead, the lithium coordination environment reveals an increasing anionic proportion via 2 cyano-moieties $N_{\text{out,TFSAM}}$ and a small contribution from 0.3 TFSAM oxygens.

When examining the underlying distribution of ether oxygen coordination numbers $\text{CN}_{O_{\text{PEO}}}$ in Figure 3f, we see that not only is the crown-ether like wrapping of lithium partly suppressed by the presence of the anion but also that a quarter of the lithium ions is entirely liberated from the polymer host (see inset in Figure 3f).

To this end, the coordination analysis indicates that the strongly coordinating TFSAM anion induces a decoupling of lithium from the polymer which, in turn, might contribute to

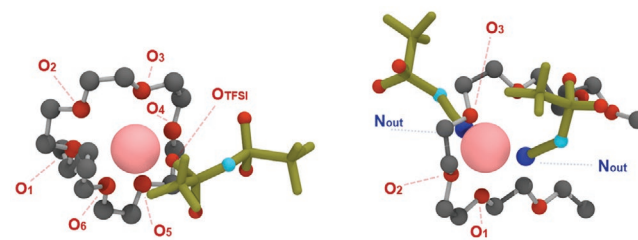


Figure 4. Snapshots depicting the average lithium coordination environment in the respective electrolyte mixture, that is, the TFSI-based (left) and TFSAM-based (right) polymer electrolyte. For reasons of clarity, only the coordinating section of the polymer chain is displayed and the anion backbones are shown in green. Carbon atoms are depicted in black, oxygen atoms in red, TFSAM's cyano nitrogen atoms in dark blue, and the anions' central nitrogen atoms in sky blue. The lithium coordinating atoms are labeled additionally.

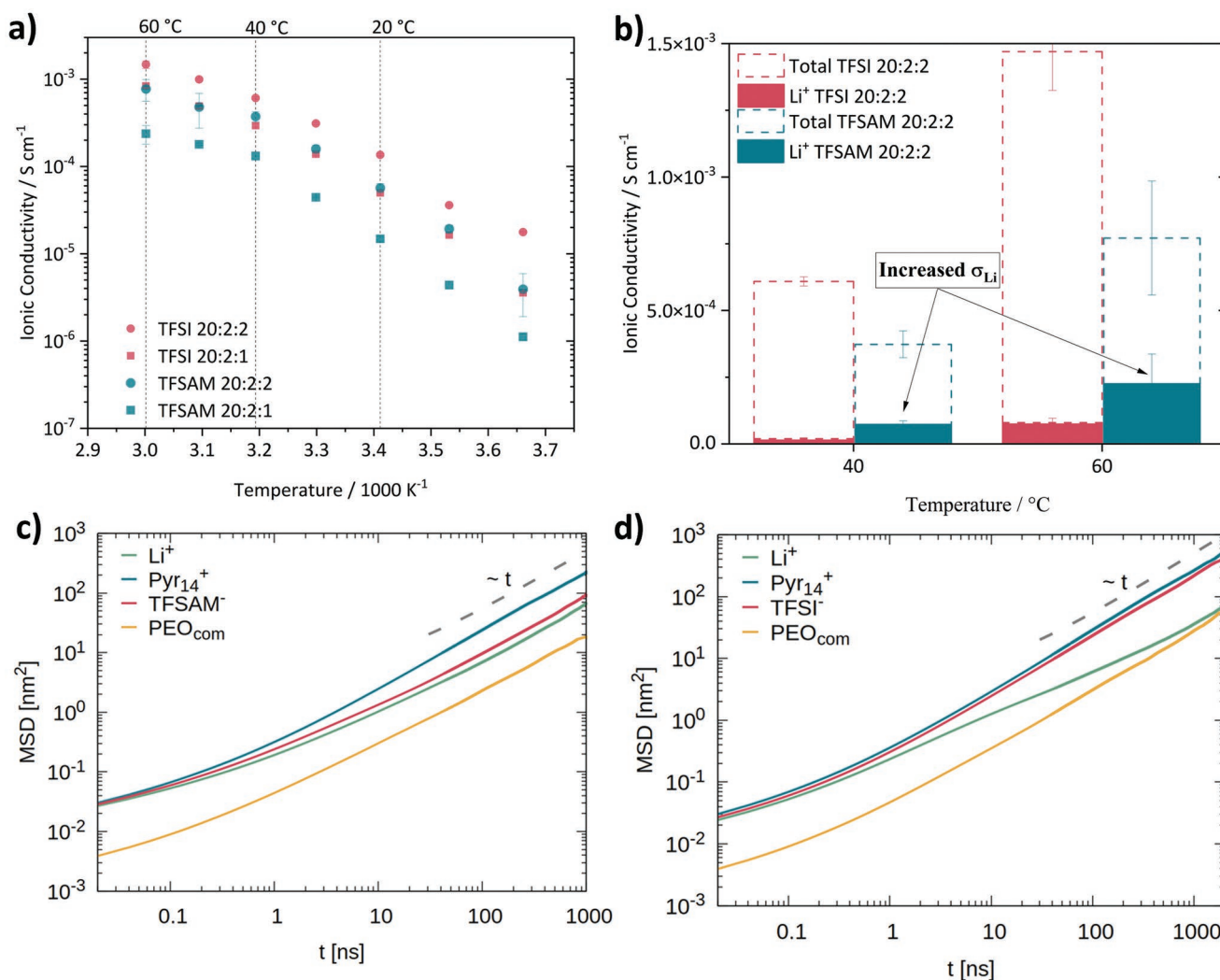


Figure 5. Top row: a) Temperature-dependent ionic conductivities of TFSAM and TFSI-based ternary electrolytes with PEO:salt:IL ratios 20:2:1 and 20:2:2; b) total ionic conductivity and portion of the conductivity contributed by Li^+ at 40 °C and 60 °C; bottom row: mean squared displacements of all molecular constituents in c) the TFSI-based and d) the TFSAM-based mixture.

a higher chain flexibility and could rationalize the lower glass transition temperatures observed for the TFSAM containing membranes.

2.5. Transport Properties: Ionic Conductivity, Li^+ Transference Numbers, Li^+ Conductivity

As TFSAM changes the coordination sphere of Li^+ in PEO-based TSPEs, it is worth investigating how this influences the dynamic processes. With regard to the application of TSPEs in lithium batteries, the Li^+ transport properties as well as the actual transport mechanism are of high interest.

The ionic conductivities of membranes with PEO:salt:IL ratios of 20:2:1 and 20:2:2 are shown in **Figure 5a**. As usually observed, a higher fraction of IL in the membrane leads to an increase in conductivity. Moreover, it can be seen that TFSAM-based electrolytes have lower conductivities than TFSI analogs, for instance at 40 °C: 6.1 mS cm^{-1} for TFSI 20:2:2 versus

3.7 mS cm^{-1} for TFSAM 20:2:2 and 2.9 mS cm^{-1} for TFSI 20:2:1 versus 1.3 mS cm^{-1} for TFSAM 20:2:1. However, considering the lithium battery application, the mobility of Li^+ is a more crucial factor than the total ionic conductivity of the electrolyte.

Therefore, the Li^+ transference numbers (t_{Li^+}) of the membranes are determined via the Bruce and Vincent method.^[34–36] As displayed in **Table 1**, t_{Li^+} is increased drastically when switching the anion from TFSI to TFSAM, for example, at 40 °C, a more than sixfold increase from 0.03 to 0.20 (the values for TFSI are coherent with results derived from both electrochemical

Table 1. Electrochemically measured Li^+ transference numbers of TFSAM and TFSI-based TSPEs with a PEO:salt:IL ratio of 20:2:2.

Temperature [$^{\circ}\text{C}$]	Li^+ transference number	
	TFSI 20:2:2	TFSAM 20:2:2
40	0.03 \pm 0.01	0.20 \pm 0.01
60	0.05 \pm 0.01	0.29 \pm 0.06

and PFG-NMR measurements on a TFSI 20:2:2 membrane ($t_{\text{Li}^+} \approx 0.05$), with half the IL content^[13].

The transference numbers were used to calculate the fraction of the ionic conductivity corresponding to lithium ions (σ_{Li^+}) via Equation (3):

$$\sigma_{\text{Li}^+} = \sigma_{\text{total}} \times t_{\text{Li}^+} \quad (3)$$

with σ_{total} being the total ionic conductivity of the TSPEs. Figure 5b illustrates how the change from TFSI to TFSAM improves σ_{Li^+} in the membrane; although, the total ionic conductivity is lower. As mentioned earlier, in the case of TFSI, the effects of the introduction of the IL to PEO-based polymer electrolytes is well-known: The IL acts mostly as plasticizer, making the polymer segments more mobile; and thus, increasing conductivity and Li^+ mobility,^[16,37] while direct Li–TFSI interactions are very limited within these TSPEs.^[38] Therefore, with TFSI-based ILs as plasticizers, the Li^+ transport is increased (compared to PEO–salt “dry” polymer electrolytes) but the usual transport mechanisms for Li^+ remain the same. Keeping this in mind, it becomes clear that the introduction of TFSAM-based ILs affects the conductivity and the Li^+ transport in TSPEs in a completely different way that results in the drastic increase of t_{Li^+} and σ_{Li^+} . So, it is safe to assume that the unilateral Li–anion coordination of TFSAM changes the whole transport mechanism for Li^+ in PEO-based TSPEs, and that this change is beneficial and leads to enhanced Li^+ mobility.

The transport characteristics of all species are probed by the mean-squared displacements (MSDs) with a larger MSD implying faster dynamics (Equation (4)):

$$\text{MSD}_i(t) = \langle (\bar{r}_i(t + t_0) - \bar{r}_i(t_0))^2 \rangle \quad (4)$$

where $\langle \dots \rangle$ denotes the ensemble average over all particles of species i and possible starting times t_0 . Due to the highly viscous nature of the electrolyte mixtures, the simulation time required to reach the diffusive regime, *that is*, $\text{MSD}_i(t) \propto t$, is considerably long. As MSDs are related to the self-diffusion coefficients D_i through the Einstein relation $D_i = \lim_{t \rightarrow \infty} \text{MSD}_i(t)/6t$, the qualitative ranking of the diffusivities can be deduced from the slopes of the respective MSD_i at long times.

Figure 5c,d displays the $\text{MSD}_i(t)$ of the center-of-mass (com) of all species in both electrolytes. In the TFSI-containing electrolyte, the diffusivities rank as $D_{\text{PyrTf}} > D_{\text{TFSI}^-} > D_{\text{Li}^+} \gtrsim D_{\text{PEO,com}}$. It is commonly found in the polymer electrolyte literature that lithium dynamics are strongly coupled to that of the polymer segments,^[16,33,37,39] which is reflected in the approach of MSD_{Li^+} and $\text{MSD}_{\text{PEO,com}}$ at long times. Note, however, that for very long times, the Li^+ dynamics exceeds that of PEO due to Li^+ transfer between distinct PEO chains.

Interestingly, a different picture emerges with the TFSAM anion for which the ranking is qualitatively maintained $D_{\text{PyrTf}} > D_{\text{TFSAM}^-} \gtrsim D_{\text{Li}^+} > D_{\text{PEO,com}}$. However, the lithium mobility shifted up toward that of TFSAM and is therefore substantially enhanced in comparison to the polymer chains. In the context of the structurally indicated lithium-polymer uncoupling, the similar lithium and TFSAM diffusivities suggest their collective motion. This assumption is further corroborated by the comparison of mean binding times τ_{Li^+-X} of Li^+ to either a distinct

Table 2. Mean residence times τ_{Li^+-X} of Li^+ with a specific TFSI or TFSAM molecule or a distinct PEO chain. τ_{Li^+-X} is evaluated from the respective residence time autocorrelation function (ACF) which probes the probability $p_{\text{Li}^+-X}(t)$ that a Li^+-X pair is preserved after time t . The ACF is fitted by a stretched-exponential decay whose integral yields an estimate of the average binding time.^[24]

	$\tau_{\text{Li}^+-\text{anion}}$	$\tau_{\text{Li}^+-\text{chain}}$
TFSI system	3.2 ns	1171.9 ns
TFSAM system	32.1 ns	75.6 ns

anion or polymer chain. As shown in **Table 2**, the introduction of the strongly coordinating TFSAM anion results in a dramatic shift of anion versus polymer host-related time scales: whereas the time a distinct Li^+ spends on average in the neighborhood of the same anion is increased by a factor 10 in the TFSAM electrolyte; the binding time to a distinct PEO chain drops to less than 10% compared to the TFSI system. This suggests that the long-range lithium transport in the TFSAM-based electrolyte is substantially aided by frequent lithium inter-chain transfers.

With these additional insights, a novel transport mechanism can be proposed: **Figure 6** displays the discovered change to the “anion-assisted” Li^+ transport when using a coordinating anion like TFSAM. As described above, the introduction of TFSAM loosens the PEO–Li coordination (observable in the shorter mean resistance times, the changed coordination sphere, and the higher Li^+ mobility (MSD)). As displayed in the scheme, Li^+ inter-chain transport is now enhanced (deduced from the mean residence times and MSDs). Moreover, this “anion-assisted” Li^+ transport is faster than in a TFSI-based TSPE (shown in the t_{Li^+} and σ_{Li^+} and in the MSDs).

2.6. TFSAM-Based TSPEs in Lithium Metal Polymer Cells

The applicability of TSPEs incorporating TFSAM was tested in LMPBs: as one of the advantages of PEO-based electrolytes is the ability to form an effective stable solid electrolyte interphase on lithium metal,^[40] this is the obvious anode material of choice for this study, also with regard to the recent trend to “revive” lithium metal as next generation anode.^[41,42] When it comes to cathode materials, it seems that in practical applications, the electrochemical stability of PEO is still the limiting factor.^[40,43] Therefore, this proof of concept was carried out in LFP||Li metal cells and compared to TFSI-based LFP||Li cells tested in parallel. **Figure 7a** shows the specific capacity evolution and Coulomb efficiency of the cells over 300 cycles.

Cells with TFSAM-based TSPEs show, on average, a slightly higher first cycle efficiency of 99.4%, whereas those with TFSI-based TSPEs are $\approx 99.0\%$, which is close but does not reveal any particular instability of TFSAM versus TFSI. Over the course of 300 cycles at C/2, TFSAM demonstrates an advantage in terms of capacity retention with 86% of the initial capacity (at cycle 300, compared to the 5th cycle), over TFSI with an 82% capacity retention. It can be mentioned that, especially within the first 50 cycles, the capacity decay differs between the two systems, with the TFSI cells losing capacity faster. However, upon further cycling, the cells with TFSI seem to stabilize and adopt a similar capacity

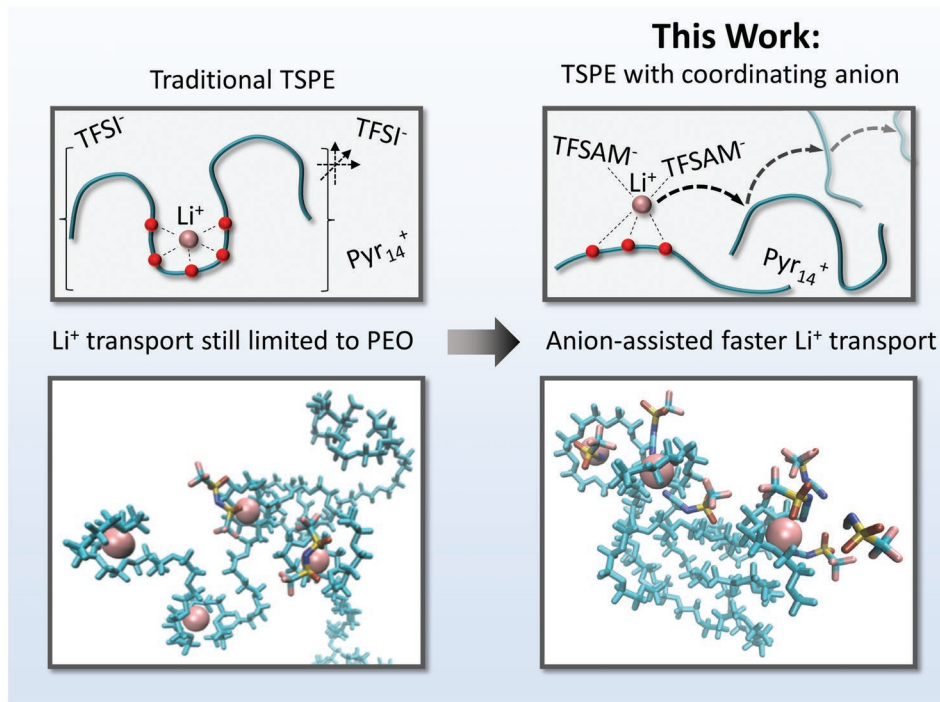


Figure 6. Novel, faster ‘anion-assisted’ transport mechanism (TFSAM-based) compared to the traditional Li⁺ transport in TFSI-based TSPEs.

fading rate. In the last 100 cycles, the capacity decay is well described by a linear fit for both systems (determination coefficients: $R^2(\text{TFSI}) = 0.9998$, $R^2(\text{TFSAM}) = 0.9995$). From the steepness of this linear development (TFSI: 0.072 mAh g^{-1} per cycle, TFSAM: 0.068 mAh g^{-1} per cycle), it becomes clear that, despite the stabilization, TFSI cells still lose capacity at a faster rate than TFSAM. For a more detailed insight into the cycling performance, the voltage profiles are shown in Figure 7b. In the first cycles, the Ohmic drop (ΔV) is higher for TFSAM-based electrolytes (see Tables S2 and S3, Supporting Information, for exact values of ΔV and equivalent series resistance (ESR)), which is coherent with the higher initial internal resistance of the electrolyte. However, it can be seen that, due to the faster Li⁺ transport, the TFSAM cells reach the LFP plateau faster with less sloped profiles and smaller hysteresis between charge and discharge (i.e., higher energy efficiencies). Over the course of cycling, ΔV and ESR increase for both electrolyte systems. Interestingly, this increase is faster for TFSI, leading to higher resistance values for TFSI in the long run (for example, ESR at the 300th cycle: $808 \text{ m}\Omega \text{ cm}^2$ for TFSI, and $707 \text{ m}\Omega \text{ cm}^2$ for TFSAM, respectively).

To highlight the effect of the faster Li⁺ transport, the discharge rate is increased to outline the influence of this increased Li⁺ transport at higher discharge currents. The evolution of capacity (Figure 7c) is, for the lower C-rates, rather similar for both systems. However, at the highest rate (2C), the advantage of TFSAM is quite clear as the TFSAM-based cells deliver considerably higher discharge capacities. A closer look to the voltage profiles (Figure 7d) reveals that the previously observed behavior becomes more obvious as the current increases: in spite of a slightly higher ohmic drop and ESR

(see Supporting Information), TFSAM reaches the LFP plateau faster with less sloped discharge curves and higher capacities at high rates.

3. Conclusion

We propose in this study the use of Li⁺-coordinating anions to accelerate the lithium ion transport in ternary PEO-based polymer electrolytes. The unilateral and strong Li–TFSAM interaction seen for the liquid binary IL-based electrolyte emerges as highly beneficial in combination with a PEO host matrix. Whereas the weakly coordinating TFSI might constitute the better anion choice in conventional liquid electrolyte formulations, it concedes the lithium ions to the rather immobile polymer, which entangles around the Li⁺ resulting in a strong coupling of the lithium dynamics to its segmental mobility, which results in slow lithium transport. Through using a strongly lithium-coordinating anion such as TFSAM, MD simulations revealed that it is not only possible to strip the lithium ions from the PEO structure but also to re-couple their dynamics from the polymer matrix to the anion. The experimental results, in turn, indicate a substantial enhancement of the lithium-ion-carried conductivity due to this structural and dynamical shifting: With TFSAM (compared to TFSI), t_{Li^+} is increased by the factor six which leads to a tripling of σ_{Li^+} despite a lower overall conductivity.

Last of all, we demonstrated that the principle of coordinating anions in TSPEs can be applied in LMPB cells. In LFP||Li metal cells, TFSAM showed a clear beneficial influence on the capacity retention (after 300 cycles: TFSAM: 86%, TFSI: 82%). Furthermore, the accelerated Li⁺ transport was visible in

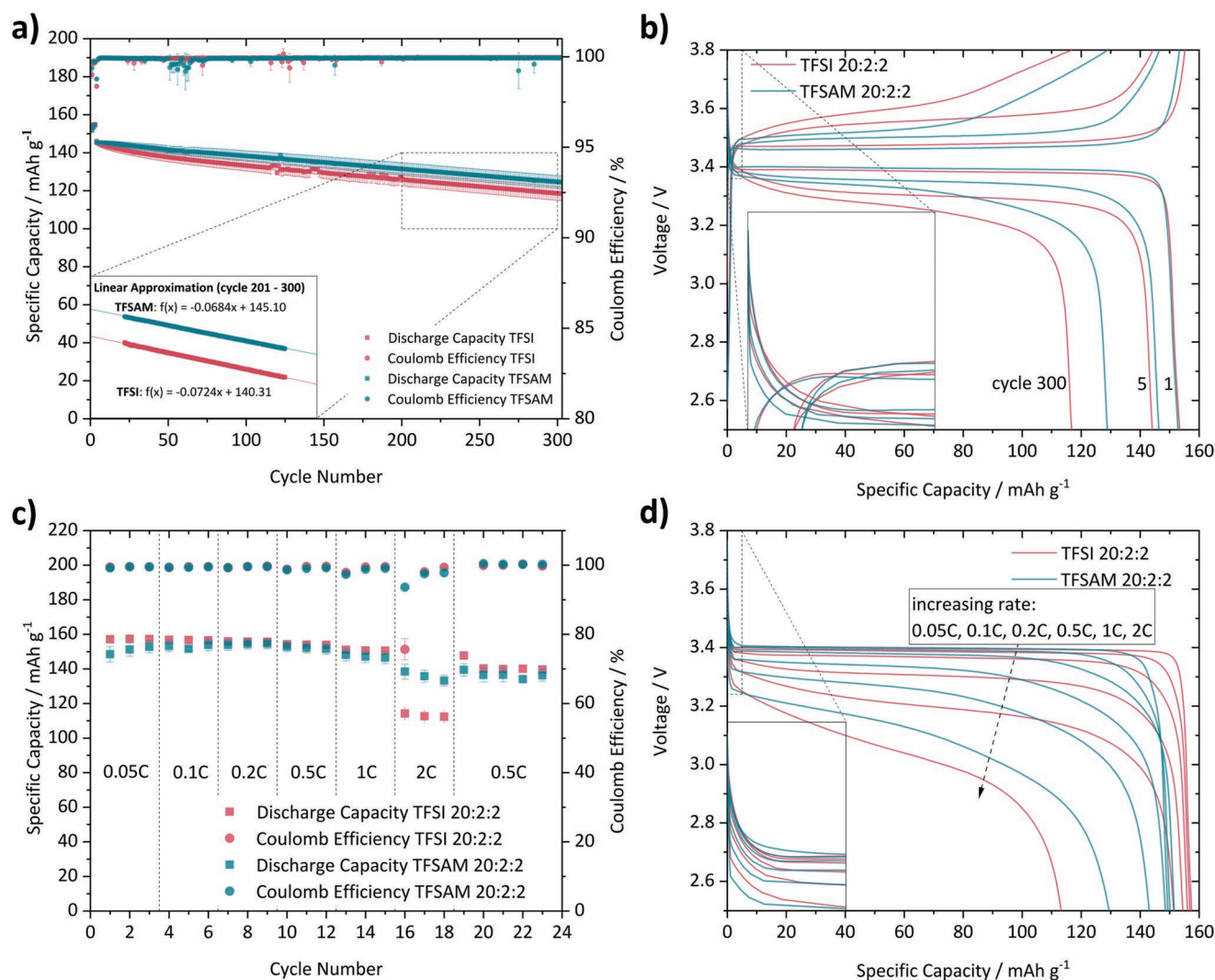


Figure 7. a) Galvanostatic cycling (300 cycles) of LFP||Li metal cells with TFSI and TFSAM-based TSPes; three formation cycles: C/10, then C/2; mass loading: 1.1 mg cm⁻²; three cells per material for error calculation; b) voltage profiles of selected charge and discharge curves of the long-term cycling (300 cycles); c) galvanostatic cycling (rate-performance test) of LFP||Li metal cells with TFSI and TFSAM based TSPes; charge rate: C/10, increasing discharge rate: C/20 to C/10, C/5, C/2, 1C, 2C, then back to C/2 (charge and discharge); mass loading: 1.1 mg cm⁻²; d) voltage profiles of selected discharge curves of the rate-performance test, third cycle of each C-rate shown.

the latter voltage profiles and higher capacities at high rates (2C).

These results recommend a rethinking of the role of coordinating anions in ternary polymer electrolytes and might lead to numerous future advances in this field of research as many anions have been proposed over the years and did not make the cut for a competitive use as either liquid electrolyte (in organic solvent-based or IL-based electrolytes) or in “dry” SPEs due to insufficient salt dissociation.

4. Experimental Section

Materials: The following materials were used in this study: Polyethylene oxide (PEO, 5 m, Sigma–Aldrich), lithium bis(trifluoromethanesulfonyl) imide (LiTFSI, Sigma–Aldrich, 99.95%), lithium (2,2,2-trifluoromethanesulfonyl)-N-cyanoamide (LiTFSAM, Provisco CS, 99%), N-butyl-N-methyl pyrrolidinium bis(trifluoromethanesulfonyl)imide (Pyr₁₄TFSI, Solvionic

SA, 99.9%), N-butyl-N-methyl pyrrolidinium dicyanamide (Pyr₁₄DCA, Solvionic SA, 99.9%), lithium iron phosphate (LFP, Südchemie), polyvinylidene fluoride (PvDF 5140, Solef), Super P carbon black (Imerys), and lithium metal foil (Albemarle, batterie grade, thickness: 50 μm).

Nbutyl-N-methyl-pyrrolidinium (2,2,2trifluoromethyl-sulfonyl)-N-cyanoamide (Pyr₁₄TFSAM) and lithium dicyanamide (LiDCA) were prepared and purified as published earlier.^[17]

Electrolyte Preparation: All components were dried under high vacuum (10⁻⁷ mbar) and, respectively (LiTFSI: 100 °C, 3 d; LiTFSAM and LiDCA: 80 °C, 5 d; Pyr₁₄TFSI: 100 °C, 5 d; Pyr₁₄TFSAM and Pyr₁₄DCA: 80 °C, 7 d; PEO: 50 °C, 7 d) before use. All electrolyte preparation was done in a dry atmosphere (dry room: dew point <-65 °C; <5.3 ppm H₂O).

Binary Liquid Electrolytes: For the formulation of IL-based electrolytes, the desired molar fraction of lithium conducting salt was dissolved in the ionic liquid with the same anion, by stirring at 50 °C.

PEO-Based Ternary Polymer Electrolytes: For the preparation of the polymer and plasticized polymer, electrolytes procedures from the literature^[6,44,38] were modified as follows: The lithium salt was mixed with the polyethylene oxide in the desired ratio by manually mixing

with a mortar and pestle. Then, (for TSPEs) the IL was added to the blended solids and all components were thoroughly mixed. The mixture was vacuum sealed in a pouch bag and annealed at 80 °C for 72 h, then pressed in a hot-press (80 °C) to the needed thickness (100, 200 μm).

Electrode Preparation: LFP cathodes containing TSPEs were prepared following a procedure reported earlier.^[13] An electrode paste containing LFP (80.0 wt%), PvdF (7.5 wt%), carbon black (7.5 wt%), and PEO-based TSPE (5 wt%), same components and ratio as electrolyte membrane) in NMP was stirred for 24 h at RT. After stirring again at 60 °C for 1 h, the paste was coated on aluminum foil (20 μm) and then dried at 80 °C for 24 h. The electrodes were calendared, punched into 12 mm diameter disks, and dried at 80 °C and under reduced pressure (10⁻³ mbar) for 24 h. The resulting active mass loading was 1.0 mg cm⁻²

Differential Scanning Calorimetry (DSC): The sample preparation was done under dry conditions and the measurements were done in Tzero hermetic aluminum pans on a DSC Q2000 (TA Instruments) calibrated with indium melting point at 156.60 °C. After an isothermal step at 60 °C, the sample was quenched to 150 °C. The heat ramp after the quenching (from -150 °C to 80 °C; 5 °C min⁻¹) was used to characterize the T_gs, as after quenching, the most distinct T_gs are achieved (subsequent cooling ramps [from 80 °C to 150 °C] in Figures S1 and S2, Supporting Information).

Pulse Field Gradient Nuclear Magnetic Resonance: All spectra were recorded on a BRUKER 4.7 T AVANCE III using a diff50 probe. Pulsed field gradient nuclear magnetic resonance (PFG-NMR) data were acquired with a (triply tuned ⁷Li/¹H/¹⁹F) 5 mm coil at 25 °C (±0.2 °C). A 0.25 M LiCl in H₂O solution and a 1% H₂O in D₂O with 0.1% CuSO₄ solution (“Doped Water”) were utilized for external calibration. The gradient strength was varied from 600 to 2947 G cm⁻¹ averaging up to 16 scans with a gradient pulse length δ of 1 ms and diffusion time Δ varied from 40 to 200 ms. The self-diffusion coefficients D of the lithium species were derived from a stimulated echo sequence (“diffSte”) after fitting the attenuated signal amplitude to the Stejskal–Tanner equation, which describes the case of rather ideal (“free”) isotropic diffusion:

$$I = I_0 \times \exp\left(-D\gamma^2\delta^2g^2\left(\Delta - \frac{\delta}{3}\right)\right) \quad (5)$$

with I being the signal intensity, I₀ the initial signal in the absence of a magnetic field gradient, and γ the gyromagnetic ratio. Data analysis was done with BRUKER Topspin 3.5 and BRUKER Dynamics Center 2.5.

Electrochemical and Physicochemical Investigation—Viscosity: All viscosity data of binary IL-based electrolytes were acquired with a kinematic Stabinger viscosimeter SVM 3001 from Anton Paar in a temperature range from 10 °C to 70 °C.

Electrochemical and Physicochemical Investigation—Conductivity: The ionic conductivities of the binary IL-based electrolytes were measured using an electrochemical impedance spectroscopy-based conductometer MCS 10 from BioLogic. All conductivity cells with cell constant ≈1 were calibrated with a standard 0.1 M KCl solution. The temperature was varied between -20 °C and 70 °C in steps of 5 °C.

For all ternary polymer electrolytes, the conductivities of the membranes were measured in a coin cell setup between two polished, stainless steel blocking electrodes (Ø = 16 mm). Impedance spectra at 0–60 °C were recorded using an Autolab PGSTAT302N potentiostat/galvanostat with impedance spectroscopy function (Metrohm AG). The frequency range was from 1 Hz up to 1 MHz. The thickness of the membrane was controlled before and after the measurement for calculating the cell constant.

Electrochemical and Physicochemical Investigation—Li⁺ Transference Number: Li⁺ transference numbers (t_{Li⁺}) for the ternary polymer electrolytes were determined electrochemically via the Bruce and Vincent method.^[34–36] It uses Li|electrolyte|Li symmetric cells and a combination of potentiostatic steps (chronoamperometry) and electrochemical impedance spectroscopy measurement. Symmetric Li|TSPE|Li cells (lithium metal electrodes Ø = 16 mm; TSPE Ø = 18 mm) were assembled for each membrane in a PAT-cell (EL-CELL). Each cell was rested at 60 °C for 4 days to ensure good contact and stabilized interfaces. Impedance

spectroscopy was performed between 100 mHz and 500 kHz prior to and at the end of the measurement with an amplitude of 10 mV. For the chronoamperometry, a voltage amplitude (ΔV) of 10 mV was applied until the current reached a steady state (I_{SS}).

The transference numbers were evaluated via Equation (6)

$$t_{Li^+} = \frac{I_{SS}(\Delta V - I_0 R_{f,0})}{I_0(\Delta V - I_{SS} R_{f,SS})} \quad (6)$$

with I₀ as the initial current, R_{f,0} as initial SEI resistance, and R_{f,SS} as SEI resistance in the steady state respectively. Given the uncertainty on the initial current I₀, it was calculated via impedance spectra collected right before the polarization according to Equation (7),

$$I_0 = \frac{\Delta V}{R_{el,0} + R_{f,0}} \quad (7)$$

with R_{el,0} as initial electrolyte resistance.

Electrochemical and Physicochemical Investigation—Cycling of LFP||Li Metal Cells: Galvanostatic cycling experiments with the TSPEs were performed in two-electrode^[45] pouch cells (cathode: LFP electrodes containing polymer electrolyte, Ø = 12 mm; anode: lithium metal, Ø = 13 mm) on a Maccor 4000 Battery Tester. After assembly, the cells were rested at open circuit at 60 °C for 24 h. All cycling experiments were then done at 40 °C. The cells were cycled between 2.5 and 3.8 V versus Li⁺/Li. For the long-term cycling experiments, after three formation cycles at C/10, the cells were cycled at C/2 for 300 cycles. For the rate-performance tests, the discharge current was increased every three cycles (with a constant charge current of C/10) from C/20 to C/10, C/5, C/2, 1C, 2C, then back to C/2 (charge and discharge).

Computational Methods: We performed all-atomistic molecular dynamics (MD) simulations of two polymer electrolyte mixtures using the software package GROMACS (version 2018.8).^[46–49] Both systems comprise 10 coiled PEO chains, which each contain 54 ether oxygen (EO) units as well as 54 lithium salt and 54 ionic liquid ion pairs. This aims to reproduce the experimentally investigated membrane composition PEO:salt:IL of 20:2:2. The lithium salt and Pyr₄⁺-based IL share the same anion, for which either TFSI or its asymmetric analog TFSAM is employed.

The atomic interactions of PEO were parameterized by the optimized potentials for liquid simulations all-atom (OPLS-AA) force field (FF),^[50] while the interactions of the ionic constituents, that is, Li⁺, Pyr₄⁺, and the anions TFSI and TFSAM, were modeled by the widely recognized OPLS-AA-derived CL&P force field.^[51–55]

Transport properties are commonly reported to be underestimated when employing non-polarizable force fields; however, consideration of polarization effects comes at a much greater computational cost. In order to mimic an effective charge screening in a mean-field like manner, the atomic partial charges were scaled by a uniform factor of 0.8.^[22,56–59]

The initial structures were generated using PACKMOL,^[60] which randomly distributed the molecules in a cubic cell in the gas phase. Then, the systems were relaxed by means of an equilibration scheme: after an energy minimization, the systems were pre-equilibrated at a temperature of 500 K and pressure of 1 bar for 10 ns with a time step of 0.5 fs in the NpT ensemble, where the temperature was maintained by a velocity-rescale thermostat and the pressure by a Berendsen barostat.^[61,62] Ensuing another energy minimization, the systems were cooled to 400 K and further equilibrated for 300 ns employing an increased time step of 2 fs. Prior to the production run, the systems were further propagated for 40 ns using a Parrinello–Rahman barostat to control the pressure.^[63] The subsequent production runs were carried out in the NpT ensemble at 400 K and a pressure of 1 bar by means of a ν-rescale thermostat (τ_v = 1 ps) and a Parrinello–Rahman barostat (compressibility of 4.5 × 10⁻⁵ bar⁻¹; τ_p = 5 ps). The equations of motion were integrated using the leap-frog algorithm at a time step of 2 fs and the coordinates were saved every 2 ps. The produced trajectories have a total length 2 μs. To prevent the system from drifting, that is, the accumulation of a center-of-mass (com) translational velocity, the com motion was removed at every step.

The smooth Particle–Mesh Ewald method was used to compute electrostatic interactions,^[64] relying on a grid spacing of 1 Å, as well as an interpolation-order of 6. The cut-off distances for long range electrostatic and the van der Waals interactions were both set to 14 Å, and the hydrogen bonds were constrained using the linear constraint solver (LINCS).^[65,66]

The simulations were analyzed using the GROMACS toolkit^[67] as well as customized scripts relying on the Python library MDAnalysis.^[68,69]

Supporting Information

Supporting Information is available from the Wiley Online Library or from the author.

Acknowledgements

J.-P.H. and A.W. contributed equally to this work. The research leading to these results has been partially funded by the “GrEEn” project funded by the ministry of economy, innovation, digitalization, and energy of The State North Rhine-Westphalia, Germany (ETN project number: 313-W044A). Analysis and simulations have been performed on the computing cluster PALMA2 at the University of Münster.

Open access funding enabled and organized by Projekt DEAL.

Conflict of Interest

The authors declare no conflict of interest.

Data Availability Statement

The data that support the findings of this study are available from the corresponding author upon reasonable request.

Keywords

ionic liquids, Li⁺ transport mechanism, lithium metal batteries, PEO-based polymer electrolytes

Received: August 15, 2022

Revised: September 28, 2022

Published online: November 18, 2022

- [1] J. R. Nair, L. Imholt, G. Brunklau, M. Winter, *Electrochem. Soc. Interface* **2019**, 28, 55.
- [2] C. Iojoiu, E. Paillard, in *Encycl. Electrochem.*, Wiley-VCH, Weinheim, Germany **2020**, pp. 1–49.
- [3] I. E. Kelly, J. R. Owen, B. C. H. Steele, *J. Power Sources* **1985**, 14, 13.
- [4] S. Chintapalli, R. Frech, *Solid State Ionics* **1996**, 86–88, 341.
- [5] M. Armand, F. Endres, D. R. MacFarlane, H. Ohno, B. Scrosati, *Nat. Mater.* **2009**, 8, 621.
- [6] J. H. Shin, W. a. Henderson, S. Passerini, *Electrochem. Commun.* **2003**, 5, 1016.
- [7] J.-H. Shin, W. a. Henderson, S. Passerini, *J. Electrochem. Soc.* **2005**, 152, A978.
- [8] J.-H. Shin, W. a. Henderson, S. Passerini, *Electrochem. Solid-State Lett.* **2005**, 8, A125.

- [9] S. Sylla, J. Y. Sanchez, M. Armand, *Electrochim. Acta* **1992**, 37, 1699.
- [10] M. Doyle, T. F. Fuller, J. Newman, *Electrochim. Acta* **1994**, 39, 2073.
- [11] K. M. Diederichsen, E. J. McShane, B. D. McCloskey, *ACS Energy Lett.* **2017**, 2, 2563.
- [12] E. Paillard, C. Iojoiu, F. Alloin, J. Guindet, J.-Y. Sanchez, *Electrochim. Acta* **2007**, 52, 3758.
- [13] J. Atik, D. Diddens, J. H. Thienenkamp, G. Brunklau, M. Winter, E. Paillard, *Angew. Chem., Int. Ed.* **2021**, 133, 12026.
- [14] L. O. Valøen, J. N. Reimers, *J. Electrochem. Soc.* **2005**, 152, A882.
- [15] M. Wetjen, G. T. Kim, M. Joost, M. Winter, S. Passerini, *Electrochim. Acta* **2013**, 87, 779.
- [16] D. Diddens, A. Heuer, *J. Phys. Chem. B* **2014**, 118, 1113.
- [17] J. P. Hoffknecht, M. Drews, X. He, E. Paillard, *Electrochim. Acta* **2017**, 250, 25.
- [18] J. Atik, J. H. Thienenkamp, G. Brunklau, M. Winter, E. Paillard, *Electrochim. Acta* **2021**, 398, 139333.
- [19] T. G. Fox, P. J. Flory, *J. Appl. Phys.* **1950**, 21, 581.
- [20] A. S. Shaplov, E. I. Lozinskaya, P. S. Vlasov, S. M. Morozova, D. Y. Antonov, P.-H. Aubert, M. Armand, Y. S. Vygodskii, *Electrochim. Acta* **2015**, 175, 254.
- [21] J.-P. Hoffknecht, J. Atik, C. Krause, J. Thienenkamp, G. Brunklau, M. Winter, E. Paillard, *Green Chem.* **2021**, 23, 9935.
- [22] Q. Huang, T. C. Lourenco, L. T. Costa, Y. Zhang, E. J. Maginn, B. Gurkan, *J. Phys. Chem. B* **2019**, 123, 516.
- [23] P. Nürnberg, E. I. Lozinskaya, A. S. Shaplov, M. Schönhoff, *J. Phys. Chem. B* **2020**, 124, 861.
- [24] A. Wettstein, D. Diddens, A. Heuer, *Phys. Chem. Chem. Phys.* **2022**, 24, 6072.
- [25] J. C. Lassègues, J. Grondin, C. Aupetit, P. Johansson, *J. Phys. Chem. A* **2009**, 113, 305.
- [26] P. C. Trulove, Electrochemical Society, **2000**.
- [27] T. R. Jow, K. Xu, O. Borodin, M. Ue, *Electrolytes for Lithium and Lithium-Ion Batteries*, Springer, New York, NY **2014**.
- [28] M. Egashira, S. Okada, J. I. Yamaki, D. A. Dri, F. Bonadies, B. Scrosati, *J. Power Sources* **2004**, 138, 240.
- [29] M. Egashira, S. Okada, J. I. Yamaki, N. Yoshimoto, M. Morita, *Electrochim. Acta* **2005**, 50, 3708.
- [30] E. Paillard, Q. Zhou, W. A. Henderson, G. B. Appetecchi, M. Montanino, S. Passerini, *J. Electrochem. Soc.* **2009**, 156, A891.
- [31] N. S. Vrandečić, M. Erceg, M. Jakić, I. Klarić, *Thermochim. Acta* **2010**, 498, 71.
- [32] R. Matsuoka, M. Shibata, K. Matsuo, R. Sai, H. Tsutsumi, K. Fujii, Y. Katayama, *Macromolecules* **2020**, 53, 9480.
- [33] D. Diddens, E. Paillard, A. Heuer, *J. Electrochem. Soc.* **2017**, 164, E3225.
- [34] J. Evans, C. A. Vincent, P. G. Bruce, *Polymer* **1987**, 28, 2324.
- [35] P. G. Bruce, C. A. Vincent, *J. Electroanal. Chem.* **1987**, 225, 1.
- [36] P. G. Bruce, J. Evans, C. A. Vincent, *Solid State Ionics* **1988**, 28–30, 918.
- [37] D. Diddens, A. Heuer, *ACS Macro Lett.* **2013**, 2, 322.
- [38] M. Joost, M. Kunze, S. Jeong, M. Schönhoff, M. Winter, S. Passerini, *Electrochim. Acta* **2012**, 86, 330.
- [39] D. Diddens, A. Heuer, O. Borodin, *Macromolecules* **2010**, 43, 2028.
- [40] I. Osada, H. De Vries, B. Scrosati, S. Passerini, *Angew. Chem., Int. Ed.* **2016**, 55, 500.
- [41] T. Placke, R. Kloepsch, S. Dühnen, M. Winter, *J. Solid State Electrochem.* **2017**, 21, 1939.
- [42] M. Winter, B. Barnett, K. Xu, *Chem. Rev.* **2018**, 118, 11433.
- [43] M. Wetjen, G. T. Kim, M. Joost, G. B. Appetecchi, M. Winter, S. Passerini, *J. Power Sources* **2014**, 246, 846.
- [44] J.-H. Shin, W. A. Henderson, C. Tizzani, S. Passerini, S.-S. Jeong, K.-W. Kim, *J. Electrochem. Soc.* **2006**, 153, A1649.
- [45] R. Nölle, K. Beltrop, F. Holtstiege, J. Kasnatscheew, T. Placke, M. Winter, *Mater. Today* **2020**, 32, 131.
- [46] D. Van Der Spoel, E. Lindahl, B. Hess, G. Groenhof, A. E. Mark, H. J. C. Berendsen, *J. Comput. Chem.* **2005**, 26, 1701.

- [47] S. Páll, M. J. Abraham, C. Kutzner, B. Hess, E. Lindahl, in *Lect. Notes Comput. Sci. (Including Subser. Lect. Notes Artif. Intell. Lect. Notes Bioinformatics)*, Springer, Cham, **2015**, pp. 3–27.
- [48] M. J. Abraham, T. Murtola, R. Schulz, S. Páll, J. C. Smith, B. Hess, E. Lindahl, *SoftwareX* **2015**, 1–2, 19.
- [49] H. J. C. Berendsen, D. van der Spoel, R. van Drunen, *Comput. Phys. Commun.* **1995**, 91, 43.
- [50] W. L. Jorgensen, D. S. Maxwell, J. Tirado-Rives, *J. Am. Chem. Soc.* **1996**, 118, 11225.
- [51] K. Shimizu, D. Almantariotis, M. F. Costa Gomes, A. A. H. Pádua, J. N. Canongia Lopes, *J. Phys. Chem. B* **2010**, 114, 3592.
- [52] J. N. Canongia Lopes, J. Deschamps, A. A. H. Pádua, *J. Phys. Chem. B* **2004**, 108, 11250.
- [53] J. N. C. Lopes, A. A. H. Pádua, *J. Phys. Chem. B* **2004**, 108, 16893.
- [54] A. S. L. Gouveia, C. E. S. Bernardes, L. C. Tomé, E. I. Lozinskaya, Y. S. Vygodskii, A. S. Shaplov, J. N. C. Lopes, I. M. Marrucho, *Phys. Chem. Chem. Phys.* **2017**, 19, 29617.
- [55] J. N. Canongia Lopes, A. A. H. Pádua, *Theor. Chem. Acc.* **2012**, 131, 1.
- [56] K. D. Fong, J. Self, K. M. Diederichsen, B. M. Wood, B. D. McCloskey, K. A. Persson, *ACS Cent. Sci.* **2019**, 5, 1250.
- [57] B. Doherty, X. Zhong, S. Gathiaka, B. Li, O. Acevedo, *J. Chem. Theory Comput.* **2017**, 13, 6131.
- [58] N. Molinari, B. Kozinsky, *J. Phys. Chem. B* **2020**, 124, 2676.
- [59] A. Thum, A. Heuer, K. Shimizu, J. N. Canongia Lopes, *Phys. Chem. Chem. Phys.* **2020**, 22, 525.
- [60] L. Martinez, R. Andrade, E. G. Birgin, J. M. Martínez, *J. Comput. Chem.* **2009**, 30, 2157.
- [61] H. J. C. Berendsen, J. P. M. Postma, W. F. Van Gunsteren, A. Dinola, J. R. Haak, *J. Chem. Phys.* **1984**, 81, 3684.
- [62] G. Bussi, D. Donadio, M. Parrinello, *J. Chem. Phys.* **2007**, 126, 014101.
- [63] M. Parrinello, A. Rahman, *J. Appl. Phys.* **1981**, 52, 7182.
- [64] T. Darden, D. York, L. Pedersen, *J. Chem. Phys.* **1993**, 98, 10089.
- [65] B. Hess, H. Bekker, H. J. C. Berendsen, J. G. E. M. Fraaije, *J. Comput. Chem.* **1997**, 18, 1463.
- [66] B. Hess, *J. Chem. Theory Comput.* **2008**, 4, 116.
- [67] M. Abraham, D. Van Der Spoel, E. Lindahl, B. Hess, The GROMACS Development Team, *GROMACS User Manual Version 2018*, Royal Institute of Technology and Uppsala University, Uppsala, Sweden **2018**.
- [68] N. Michaud-Agrawal, E. J. Denning, T. B. Woolf, O. Beckstein, *J. Comput. Chem.* **2011**, 32, 2319.
- [69] R. J. Gowers, M. Linke, J. Barnoud, T. J. E. Reddy, M. N. Melo, S. L. Seyler, J. Domanski, D. L. Dotson, S. Buchoux, I. M. Kenney, O. Beckstein, in *15th PYTHON Sci. Conf. (SCIPY 2016)*, Los Alamos National Lab. (LANL), Los Alamos, NM (United States), Austin, Texas, United States, **2016**.
- [70] J. Patrik, P. Gejji Shridhar, T. JoËrgen, L. Jan, *Electrochim. Acta* **1998**, 43, 1375.
- [71] K. Fujii, T. Fujimori, T. Takamuku, R. Kanzaki, Y. Umeyayashi, S. I. Ishiguro, *J. Phys. Chem. B* **2006**, 110, 8179.